**Electron magnetic resonance in heterogeneous photocatalysis research**

(Article begins on next page)

# Electron Magnetic Resonance in heterogeneous photocatalysis research.

**Mario Chiesa, Elio Giamello\*, Stefano Livraghi, Maria Cristina Paganini, Valeria Polliotto, Enrico Salvadori**

Dipartimento di Chimica, Università di Torino, Via P. Giuria 7, 10125., Torino (Italy)

 E-mail: elio.giamello@unito.it

## Abstract

The contribution of Electron Magnetic Resonance techniques, and in particular of CW-EPR, to the experimental research on photocatalytic phenomena is illustrated in this paper with selected examples. In the first part of the paper the role of EPR in unravelling the nature and the features of extrinsic point defects in semiconducting oxides is epitomized using the important example of the photoactive nitrogen center in various semiconducting oxides. In the second part we describe how EPR can monitor the processes that follow the initial photoinduced charge separation in photocatalysis, namely the stabilisation, migration and surface reactivity of electrons and holes. Finally, we will discuss how the role of EPR in photocatalysis is not limited to monitor phenomena occurring in the solid or at its surface but it can be extended to the investigation of the liquid phase by employing the spin trapping techniques to monitor the nature and the concentration of the reactive free radicals formed along the photocatalytic process.

Keywords: EPR, photocatalysis, paramagnetic defects, oxides

## 1.    Introduction

   The literature in the area of photocatalysis applied to pollutants remediation [1, 2] is largely dominated by studies focused on the reactivity and the efficiency of the photocatalyst under various conditions. When non-conventional photocatalyst are employed instead of benchmark systems such as the universally known P25-$TiO_2$, the characterization of the solid catalyst is very often limited to basic tools such as X-ray diffraction, optical spectroscopy and electron microscopy because the emphasis in these cases is on the results of photocatalytic activity rather than on the active species. Only a relatively minor fraction of published work pays more attention to the detailed physical mechanisms of photocatalysis with the support of advanced physical techniques. The attention to fine physical-chemical details and mechanisms usually increases in the area of heterogeneous photocatalysis and photoelectrochemistry applied to the so-called artificial photosynthesis [3, 4] concerned with water photosplitting or carbon dioxide photoreduction.

   The Electron Paramagnetic Resonance  (EPR) technique is not unknown in the area of photocatalysis even though, due to their capability to monitor states containing unpaired electrons, one would expect a more intense application of such techniques in this field, in analogy to what has been done in the past in the area of natural photosynthesis [5-7].

Recently, beside the classic EPR acronym, the broader EMR (Electron Magnetic Resonance) has been introduced in analogy with the well known NMR one, employed for nuclear resonance. This more general term encompasses all technical approaches monitoring interactions between electron magnetic dipoles. The reason of the potentiality of EMR in photocatalytic studies is twofold. Firstly, in photocatalysis the problems of charge separation, electron transfer and radical intermediates (parallel to those occurring in natural photosynthesis) have a paramount importance. EMR measurements can be done either in the dark or under illumination with light of various frequencies providing the great advantage of observing the photocatalytic system under working conditions. Secondly, electron magnetic resonance is extremely useful to monitor (paramagnetic) defects in the solid state and it is well known how intrinsic and extrinsic defects in the solid can influence both light absorption and charge recombination [8-13].

The present paper is devoted to illustrate, with selected examples, the potential of electron magnetic resonance, and in particular of the classic technique of Continuous Wave Electron Paramagnetic Resonance - CW-EPR - in the area of photocatalysis based on semiconducting oxides. It is organized as follows: The first part briefly illustrates the basic principle of EPR and the main features of the spectra of polycrystalline solids. The second part deals with applications of CW-EPR to photocatalytic solids considering phenomena of charge carriers' stabilization, surface reactivity of carriers and identification of photoactive defects in the solid. A short final section is devoted to spin trapping, an EPR application aimed to monitor the presence of photogenerated reactive radicals in solution.

## 2. EMR techniques.

The conventional CW-EPR is, among the various EMR techniques, the dominant one in heterogeneous catalysis and photocatalysis studies. A great advantage of EPR is that it exclusively monitors paramagnetic systems i.e. chemical entities bearing one or more unpaired electrons and is blind to all other diamagnetic entities. In a CW-EPR experiment the system under investigation is irradiated by a continuous flow of microwaves at a fixed frequency in the presence of an applied magnetic field. When resonance conditions are fulfilled a transition occurs between two spin states of the unpaired electron(s). For instrumental and sensitivity reasons, the EPR spectra are usually reported as first derivative of the microwave absorption as a function of the swept magnetic field. The signal intensity depends on the amount of paramagnetic centers and is obtained by double integration of the first derivative trace. The most commonly used microwave frequency in the study of heterogeneous catalysts and photocatalysts is ca. 9.5 GHz or X-band.

Similarly to what was done in Nuclear Magnetic Resonance a long time ago, pulsed methods were also introduced in EPR though more recently. Pulsed EPR is based on irradiation by controlled short pulses of microwaves and various applications such as ESEEM (Electron Spin Echo Envelope Modulation) or FT-ESR (Fourier Transform Electron Spin Resonance) are based on such principle.

The EPR spectrum of a paramagnetic species can be described in terms of a spin Hamiltonian which consists in a series of energy terms corresponding to the interaction of the electron spin with its surroundings. To rationalize the results described in the following it is sufficient to consider the two first terms of a longer series (1)

$$\mathcal{H} = \beta_e \boldsymbol{S} \cdot \boldsymbol{g} \cdot \boldsymbol{B} + \boldsymbol{S} \cdot \boldsymbol{A} \cdot \boldsymbol{I} \qquad (1)$$

The first term is the electronic Zeeman operator which accounts for the interaction of the electron spin S with the external magnetic field $\boldsymbol{B}$, $\beta_e$ being the Bohr magneton. The interaction is determined

by the **g** tensor, a 3x3 matrix which, in general, can be reduced to its diagonal form. In this case $g_{xx}$, $g_{yy}$, $g_{zz}$ are the principal elements of the tensor whose values depend on the electronic structure of the ground and excited states of the paramagnetic species. In the absence of other interactions (electron-nucleus, electron-electron) the g matrix determines the resonance values i.e. the magnetic field at which the resonance occurs for a given orientation of the paramagnetic species in the magnetic field itself. In the case of powdered system with random orientation of a huge number of crystallites the shape of the "powder spectrum" is isotropic and contains, in principle, all the information about the g tensor and the spectrum does not vary changing the orientation of the sample in the magnetic field. Determining the exact g values in some cases can be difficult (poor resolution, overlap of different signals etc.) and simulation of the experimental profile is therefore recommended [14]. Akin to multifrequency NMR, changing the applied magnetic field (and therefore the working microwave frequency) can be a convenient method to disentangle complex EPR spectra by exploiting differences in their characteristic g values.

The second term represents the interaction between electron spin and nuclear spins, usually referred to as hyperfine interaction. This interaction increases the complexity of the EPR spectrum however providing important information about the wavefunction of the unpaired electron (SOMO). In Eq (1) **A** is the hyperfine tensor (a 3x3 matrix again) and **I** is the nuclear spin vector. In CW-EPR the hyperfine interactions give rise to line splitting in the spectrum producing the so-called hyperfine structure. A set of $2I+1$ lines is expected (for any given orientation of the species into the magnetic field) due to the interaction of the electron spin with a nucleus having nuclear spin quantum number I. From the hyperfine matrix two types of contributions can be easily derived i.e. the Fermi contact terms ($a_{iso}$, related to electron spin density in s-type orbitals) and the dipolar term (T) related to spin density in p- or d-type orbitals. The term hyperfine interaction is usually associated to the interaction between the unpaired electron of a given species, for example a paramagnetic ion in a crystal, and the nucleus of the same species. The same magnetic interaction involving the unpaired electron and nuclei present in the surrounding is known as super-hyperfine (shf) interaction. The shf tensor, when present, provides a significant description of the environment of the magnetic center and allows to obtain a map of the spin density distribution over the various orbitals. The **g** and **A** tensors can be classified on the basis of their symmetry (for instance, an isotropic tensor has three equal principal components, an axial tensor has two components equal differing from the third) which in turn depends on the symmetry of the paramagnetic center. Figure 1 shows three schematic examples of simulated EPR powder spectra showing respectively an axial (1a), an orthorhombic signal with no hyperfine interaction (g tensor only) (1b) and the same orthorhombic signal of 1b but with added hyperfine splitting due to a nucleus with I =3/2 (four hyperfine lines) (1c).
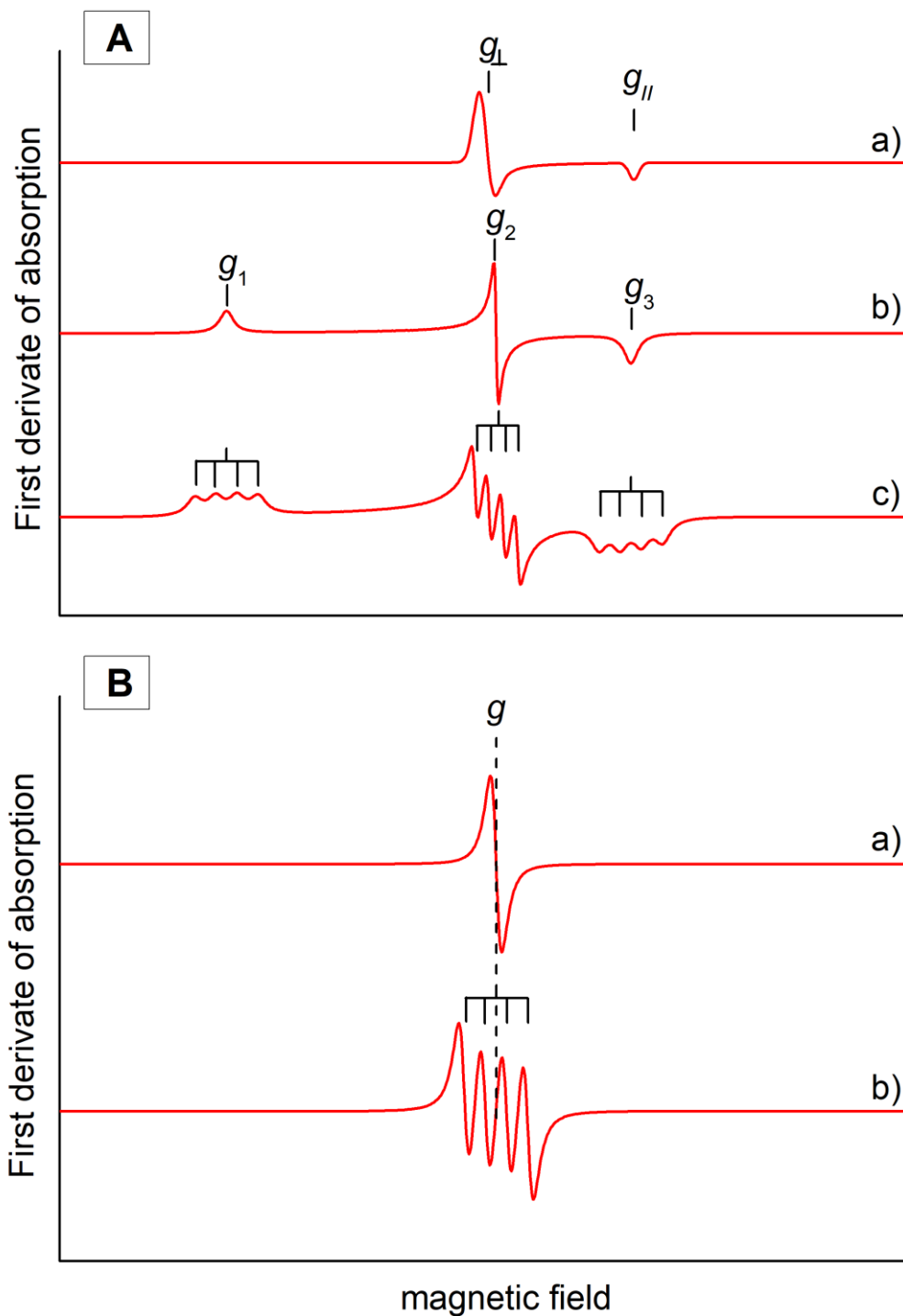
Figure. 1. Panel A. Calculated profiles (first derivative of absorption) of the EPR spectra in the case of an axial g tensor (a), a rhombic g tensor (b) in the absence of hyperfine interactions. The profile in c) is based on the g tensor of the species in b) with the onset of a hyperfine interaction with a nucleus having I=3/2 (four lines).

Panel B. Calculated profiles of solution spectra. The g and A parameters of a) and b) are those of species b) and c) in Panel A.

EPR spectra in solution are much more simple and symmetric than those in the solid state. This is because the rapid tumbling of the molecules in solution tends to average the anisotropic magnetic

interactions occurring in the system. The **g** tensor components are therefore reduced to an average value ($g_{av}$) while the dipolar component of the hyperfine tensor is averaged to zero and the only isotropic Fermi contact term ($a_{iso}$ or a) contributes to the hyperfine separation. In Figure 1, panel B (spectra a and b) we report, for comparison, two spectra simulated using the parameters of species b) and c) (panel A) respectively and imposing the free tumbling typical of a fluid solution.

## 3.    Extrinsic point defects in semiconducting oxides employed in photocatalysis.

EPR techniques are extremely powerful tools for the description of defects in solids because many types of important defects contain unpaired electrons. [15, 16] The importance of EPR in defects characterization is due to both the inherent accuracy of the technique in describing the structure and the spin density distribution of a paramagnetic center and to its high sensitivity allowing detection of small amounts of such centers.

Point defects in a solid lattice can be classifies as intrinsic, when the composition of a solid is not altered by the presence of the defect itself, and extrinsic when a chemical impurity is present (or has been purposely introduced) in the solid. Intrinsic defects such as ion vacancies are always present in a crystal lattice due to thermodynamic reasons. Their abundance however can be modified in various ways including thermal or thermochemical treatments, irradiation etc. Extrinsic defects are often introduced in the solid to modify particular physical properties. In the evolution of photocatalytic research, the use of impurities to modulate the optical properties and the whole photocatalytic performance of a solid has grown with time.

A well-known example is related to the use of nitrogen to dope semiconducting photocatalytic oxides. Nitrogen doped Titanium dioxide ($N-TiO_2$) was first reported in 2001 in a renowned paper by R. Asahi and coworkers [17] and it was described as a visible light-sensitive solid potentially active in photocatalytic processes carried out under solar light and so capable to overcome the limits of pristine $TiO_2$ whose high energy gap value (from 3.0 to 3.2 eV for the main polymorphs) implicates the use of UV frequencies [18]. The use of EPR in strict connection with computational chemistry has been decisive to understand the nature of the doped system and the fine details of the related extrinsic defect [19, 20]. Actually two types of photoactive centres have been described for $N-TiO_2$. The first one is based on substitutional nitrogen (N substitutes O in some lattice sites) and is usually formed by high temperature treatments of $TiO_2$ under ammonia atmosphere [21-25]. The more interesting defect from a photocatalysis standpoint however is regularly formed using wet chemistry preparations of the solid such as sol-gel reactions or hydrothermal synthesis [26-29]. It is based on a N atom located in an interstitial site of the structure but chemically bound to a lattice O thus forming a charged NO group in the bulk of the solid (Scheme 1) [30]. It has been demonstrated by EPR experiments under illumination that a fraction of these centers bear one electron in the SOMO and are consequently paramagnetic and EPR active. The paramagnetic fraction can be formally written as $NO^{2-}$ (however, being the sample a crystalline solid, the actual charge is of course lower than 2 since the matrix is only partially ionic) while the diamagnetic fraction, with two electrons in the HOMO, can be formally thought as $NO^{3-}$ [31]. Both these centers are responsible for the optical absorption in the visible of the doped system.

In order to illustrate all concepts discussed so far, Figure 2 compares the EPR spectra of N species in various semiconducting oxides. The first signal (Figure 2Aa) is that of $NO^{2-}$ species in $TiO_2$. The spectrum has been understood on the basis of careful computer simulation, isotopic substitution ($^{15}N$ for $^{14}N$, Figure 2Ba) and use of multi-frequency EPR [32].
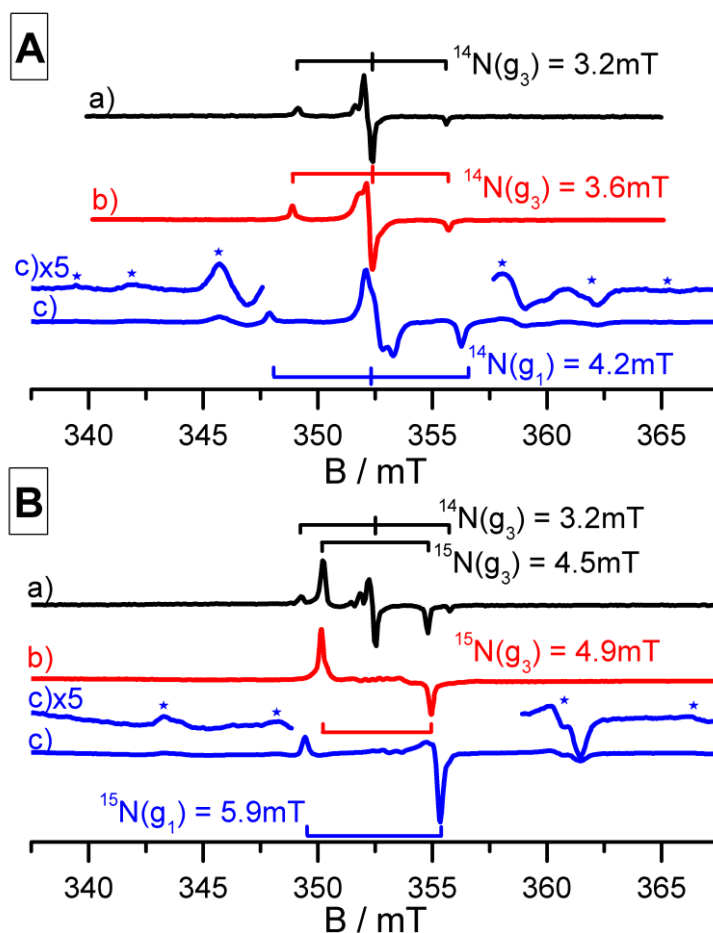
Figure 2. EPR spectra of $^{14}$N defects (panel A) and $^{15}$N defects (panel B) in various solids. a) TiO$_2$, b) ZrTiO$_4$, c) SnO$_2$. In the spectrum B a) the contribution of a minor fraction of $^{14}$N is also visible. The asterisks indicate the further splitting due to the interaction with the Sn nuclear spin.

This systematic approach has allowed precise determination of the small rhombicity of the g tensor as well as the component of the N hyperfine tensor (table 1). From the hyperfine values it could be concluded that the unpaired electron is localised on the $p$ orbital of N for 56%. The remaining spin density, as confirmed by DFT calculations, is mainly localized on $p$ orbitals of oxygen. Since $^{16}$O has zero nuclear spin it does not generate a corresponding hyperfine structure. DFT also suggests that a minor fraction of the spin density is spread on the lattice ions surrounding the paramagnetic centre. In conclusion, the whole description of the paramagnetic N defect is that of a N-O $\pi$-system with the unpaired electron in one of the two $\pi^*$ orbitals constituting an intra band gap state lying few tenths of eV above the valence band limit (Scheme 1). Irradiation of the system by a suitable visible wavelength (about 440 nm) causes the promotion of NO$^{x-}$ electrons (x = 2, 3) to the conduction band where they become available for reduction reactions.
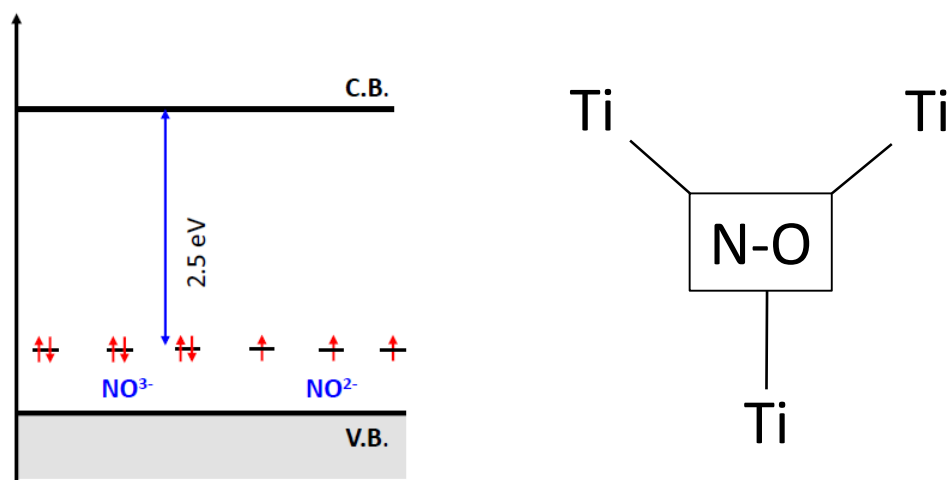
Scheme 1. Left: electronic structure of N-TiO$_2$; right: model structure for interstitial N-dopants in TiO$_2$.

Table 1. $g$ values, hyperfine (A) constants (mT) and spin density of the N centers in TiO$_2$, ZrTiO$_4$ and SnO$_2$.

| | $g_1$ | $g_2$ | $g_3$ | Nucleus | $A_1$ | $A_2$ | $A_3$ | $\rho(\%)$ | Ref |
|---|---|---|---|---|---|---|---|---|---|
| N-TiO$_2$ | 2.005 | 2.004 | 2.003 | $^{14}$N | 0.23 | 0.44 | 3.22 | 56 | [33] |
| | | | | $^{15}$N | 0.33 | 0.63 | 4.64 | | |
| N-ZrTiO$_4$ | 2.0081 | 2.0046 | 2.0038 | $^{14}$N | 0.22 | 3.40 | 0.16 | 69 | [34] |
| | | | | $^{15}$N | 0.32 | 4.90 | 0.26 | | |
| N-SnO$_2$ | 2.0053 | 2.0023 | 1.9978 | $^{14}$N | 4.17 | 0.083 | 0.078 | 80 | [35] |
| | | | | $^{15}$N | 5.88 | 0.117 | 0.110 | | |
| | | | | $^{119}$Sn | 12.2 | 12.8 | 12.4 | | |
| | | | | $^{117}$Sn | 11.7 | 12.3 | 11.9 | | |

   The features of the N centre (NO$^{2-}$) in ZrTiO$_4$, zirconium titanate [34], a solid with a structure analogous though not equal to that of the main TiO$_2$ polymorphs, are strictly similar to those discussed above and are reported in Figure 2Ab and Table 1. To show how isotopic substitution helps in determining the features of a paramagnetic centre, Figure 2B reports the spectra of the same species present in Figure 2A obtained using $^{15}$N. Since $^{15}$N has nuclear spin I = ½ the series of triplets is substituted by a series of doublets (see the stick diagram in Figure 2B) without a central line. This dramatically changes the profile of the EPR spectra.
The electron spin density on the N tom is, in this case, slightly higher than that measured in the case of N-TiO$_2$ (Table 1).
   The N defect in stannic oxide (SnO$_2$, rutile structure, Figure 2Ac and 2Bc) is here reported to show that in some case the electron density in the environment of the paramagnetic species can be monitored by EPR provided the presence of non-zero nuclear spin nuclei. In fact, while in TiO$_2$ and ZrTiO$_4$ the abundance of "magnetic" cations is insufficient to generate a detectable superhyperfine structure, in the case of SnO$_2$ the abundances of $^{117}$Sn and $^{119}$Sn (both I=1/2 and 7.68% and 8.59% natural abundance, respectively) is high enough to unravel a rich and complex hyperfine structure that enhance the complexity of the signal. Although we do not discuss the full procedure to simulate

the experimental EPR spectra we note that computations are challenging as they must take into account the statistical abundance of the various isotopomers containing respectively one, two, three and zero magnetic Sn ions around each nitrogen. Careful simulations drew the conclusion that the N center in $SnO_2$ is substitutional (N takes the place of O in the lattice, Scheme 2) as indicated by the fact that the three Sn ions surrounding the N defect are magnetically equivalent and hence structurally equivalent [35].
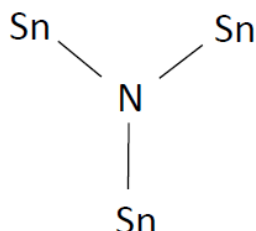


Scheme 2. Model structure for the substitutional N-dopant in $SnO_2$.

The electron spin density on nitrogen (Table 1) is in this case around 80%, definitely higher than in the case of N-$TiO_2$ and N-$ZrTiO_4$ and in line with the assignment of the EPR spectra in Figure 2c to a substitutional N center.

Nitrogen is not the only element used to modify titania and other semiconducting oxides for photocatalytic purposes. It is enough to mention the case of fluorine, boron or sulphur used as single dopants or in pairs for the so-called co-doping of photocatalytic oxides. [36-38]

## 4. EPR in heterogeneous photocatalysis.

### 4.1. Monitoring photogenerated charge carriers

The basic action of photocatalytic processes consists in the light induced charge separation occurring in a semiconductor (often a Metal Oxide, MO) caused by photons having, in most cases, energy higher than the band gap of the solid. Photon absorption causes the promotion of electrons from the valence band (VB, built up by $O^{2-}$ orbitals) to the conduction band (CB) leaving behind an electron-hole, according to the equation:

$$MO + h\nu \rightarrow h^+_{(VB)} + e^-_{(CB)} \tag{2}$$

After the initial excitation a competition starts between the two opposite processes of charge recombination (leading to the loss of the photon energy) and charge migration.

EMR techniques have nicely contributed to the investigation of the fate of photogenerated carriers in photocalytic systems as the trapping of charge carriers and their reaction at the surface of the photocatalyst usually involves the formation of a paramagnetic entity. Fundamental work in this area has been performed by Howe and Grätzel on colloidal suspensions of $TiO_2$ [39, 40] and by other groups that followed the charge carrier trapping on $TiO_2$ and other oxides [41-43] or the dynamics of charge separation [44, 45].

In the case of semiconducting oxides used in photocatalysis when the photoexcitation experiment is carried out under vacuum (i.e. in the absence of a photocatalytic process) a fraction of the photogenerated carriers can be observed either under continuous irradiation or trapped after irradiation provided that the temperature is kept low enough to prevent recombination. An example

is shown in Figure 3 in the case of two oxides with band gap higher than 3eV irradiated by UV light, ZrTiO$_4$ (Figure 3a) and ZnO (Figure 3b) respectively. In both cases the positive holes tend to localize on the oxygen ions (O$^{2-}$) of the lattice. In chemical term this can be read as the formation of a (paramagnetic) O$^{\bullet-}$ ion whose signal is observed, as expected, at low magnetic field, i.e. at g> g$_e$, being g$_e$ = 2.0023 the free spin value

$$O^{2-} + h^+ \rightarrow O^{\bullet-} \qquad (3)$$

The fate of photogenerated electrons is not exactly the same for the two metal oxides though the related signal appears in the same region of the spectrum (right-end side, g < g$_e$) [46]. In the case of ZrTiO$_4$, like in the case of TiO$_2$, the electron are trapped on metal cation sites [47].

$$Ti^{4+} + e^- \rightarrow Ti^{3+} \qquad Zr^{4+} + e^- \rightarrow Zr^{3+} \qquad (4)$$
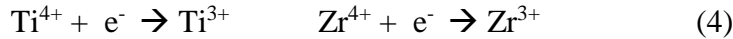
The spectral profiles of both trivalent titanium and zirconium ions are visible in Figure 3a. In particular the broad signal associated to Ti$^{3+}$ is related to ions located at the surface of the solid, the large linewidth of the signal being due to the heterogeneous environment typical of the nanoparticles surface. This particular assignment has been possible using a TiO$_2$ sample whose surface was enriched with $^{17}$O and using advanced EMR techniques, namely ESEEM (Electron Spin Echo Envelope Modulation) and HYSCORE (Hyperfine Sublevel Correlation) [48]. By this approach it has been possible to discriminate between surface and bulk Ti$^{3+}$ centers.

The narrower signal assigned to Zr$^{3+}$ [49] corresponds to stable electron traps present in the solid. After warming in fact (data not shown) the trace of the electrons trapped at titanium sites disappears because of recombination while the smaller fraction of Zr$^{3+}$ (with the corresponding holes) remain unaffected.
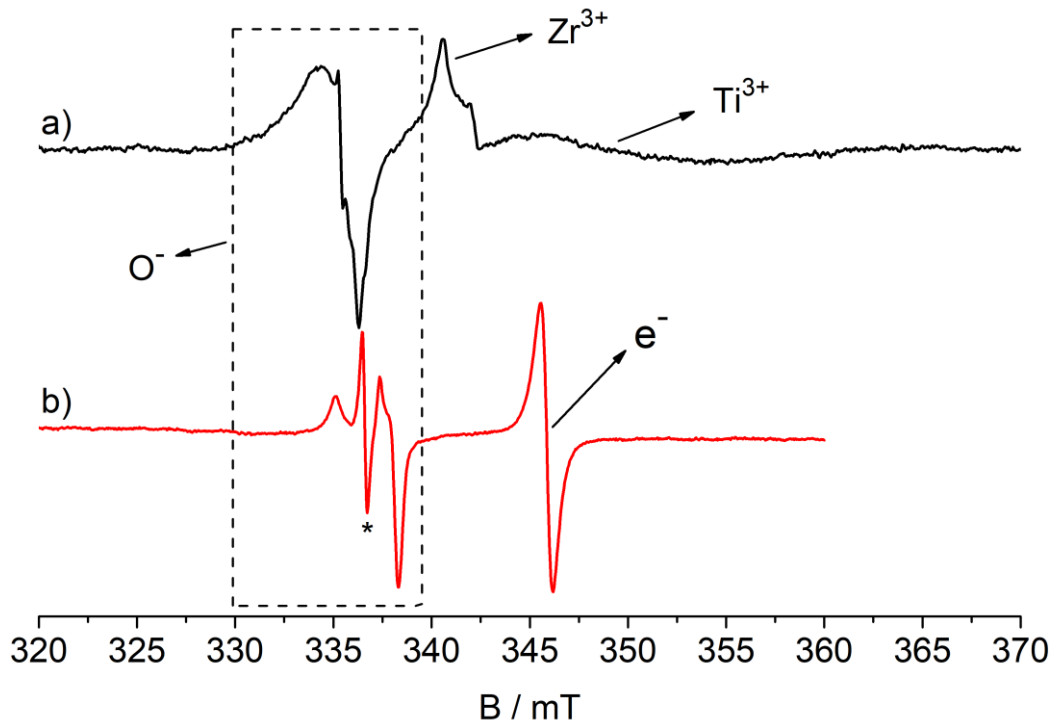


Figure 3. Charge carrier trapping in ZrTiO$_4$ (a) and ZnO (b) irradiated by UV-Visible light. Asterisks indicate spurious EPR signals. The notation e- refers to shallows donor levels (see text).

In the case of ZnO (Figure 3b) the photoexcited electrons produce a symmetric signal at g = 1.96 (about 345mT) typical of shallow energy states, at the borderline of the conduction band. The behaviour of ZnO is strongly sensitive to the preparation method adopted [50]. The result shown in the figure is related to a material prepared by precipitation from a solution of zinc acetate and sucessive calcination. Differently from the case of zirconium titanate the excited electrons, in this case, are not localized on a single ion but, rather, are mobile, contribute to the solid conducibility and can be thought as associated to the Zn orbitals forming the conduction band [51].

Experiments similar to that shown in Figure 3 can be run also employing visible frequencies not only in the case of semiconductors with band gap lower than 3 eV but also in cases of semiconductors with high band gap that have been modified in order to make them sensitive to visible light. This is the case discussed in the previous section of N doping of $TiO_2$ or that, more recently reported by our group, of oxides modified using tetravalent cerium. [52-54]

According to the nature of the oxide matrix, cerium ions can be diluted in the bulk or, in case of non-solubility, it can form aggregates of cerium dioxide in contact with the surface of the main component. The former case is that of cerium doped zirconium dioxide (Ce-$ZrO_2$) [52, 53]. In this case the structural affinity between $CeO_2$ and zirconia favour the dissolution of relatively high amounts of the former, with $Ce^{4+}$ ions regularly dispersed in the main matrix occupying the regular cationic site. The second case is that of $CeO_2$-$TiO_2$ and $CeO_2$-ZnO [54]. For both systems a complex mixed junction is formed at the boundary of the two phases.

Figure 4 compares the effect of irradiation of pristine $ZrO_2$ and Ce-$ZrO_2$ with polychromatic visible light having $\lambda > 420$ nm. Due to the wide band gap of zirconium dioxide (about 5 eV) it is obvious that no charge separation effect can occur in the case of the bare oxide (left side of Figure 4) as illustrated by the corresponding energy level diagram. At variance the Ce doped material show sensitivity to visible light as firmly indicated by the formation of the of trapped electrons ($Zr^{3+}$ ions) and trapped hole EPR signals upon irradiation (right side of the figure). This phenomenon has been interpreted, with the strong support of computational results [52], in terms of the formation of mid-band gap $Ce^{4+}$ 4f empty states with allow excitation of electrons from the valence band with low energy photons (about 2,5 eV needed). These excited electrons are likely further promoted by a second photon to the conduction band of the system thus becoming available for reduction reaction. A similar role, in the case of $CeO_2$-ZnO is played by the photoactive interface formed at the boundary between the two non-mutually soluble oxides. The photoactivity revealed by EPR experiments (Figure 4) has been further confirmed since the novel systems have been successfully used in the mineralisation of some emerging pollutants using visible light [55]. It is worth noting that the potential advantage of the systems here described with respect to semiconductors with small band gap consists in the fact that the carriers formed by visible light are, in this case, in bands having highly negative (CB) and positive (VB) potentials, in principle suited for both efficient oxidative and reductive actions respectively.
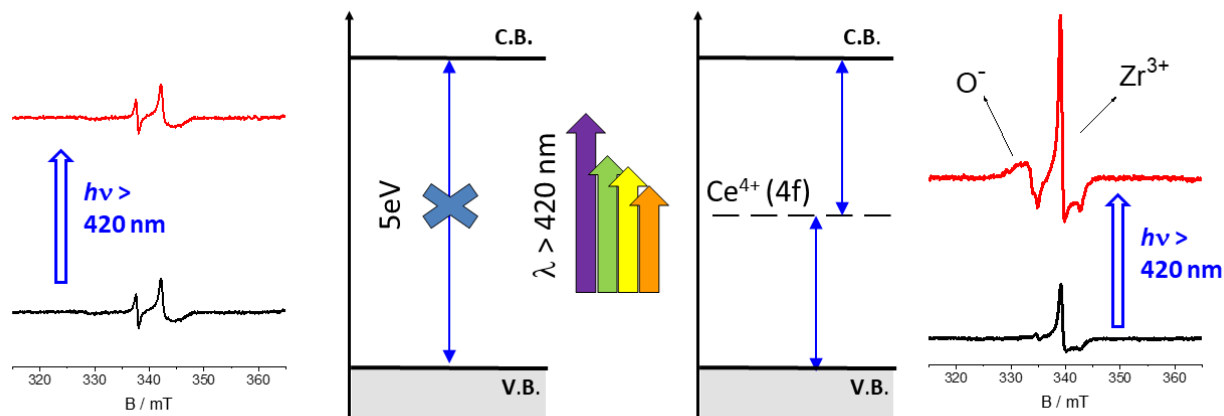
Figure 4. Effect of irradiation with polychromatic visible light having $\lambda > 420$ nm of pristine $ZrO_2$ (left) and Ce-$ZrO_2$ (right). The set of arrows in the figure compares the energy of the photons used in irradiation with the band gap of the systems.

EPR results about the stabilisation of holes in semiconducting oxides indicate that there are local factors that influence the stabilisation. Figure 5a and b reports the EPR spectra of holes trapped in fully dehydrated $TiO_2$ and $ZrO_2$. The two signals are analogous and their relatively small mutual differences reflect the difference in the symmetry of oxygen ions in the two structures. The signal in Figure 5c is due to a surface hydrated titania. It can be seen that the presence of surface hydroxyl groups and surface adsorbed water induces the formation of an extra species not observed in the case of the dehydrated material [56]. This second species, as shown by electron-nuclear double resonance (ENDOR) experiments, interacts with adsorbed water molecules [57].

A strong effect of hole localization can also be played by extrinsic defects present in the solid. This is shown comparing the spectra of irradiated $TiO_2$ and $ZrO_2$ (Figure 5a and 5b) with those of the same oxides doped with about 5% of Al (Figure 5d and 5e). Al ions in the $MeO_2$ network induce the formation of oxygen vacancies to compensate the charge unbalance. The as-prepared systems thus contain oxygen vacancies and are diamagnetic. The large majority of holes ($O^{\bullet-}$) formed upon irradiation are stabilized in close proximity of an Al ion as indicated by the hyperfine structure visible in spectra 5d and 5e (the $^{27}$Al nucleus – 100% of natural abundance – has a nuclear spin I=5/2 which produces three sets of 6 lines for each g component). The nice hyperfine structure observed in the spectra coupled with DFT calculations allows the description of the trapping site as an oxygen ion coordinated by three metal cations one of which is an $Al^{3+}$ ion (Scheme 3). The value of the $a_{iso}$, the Fermi contact atomic term for Al, is large enough to generate a well resolved hyperfine structure even with a very small spin density delocalization on Al ions.
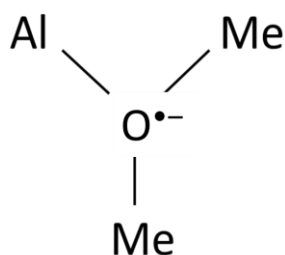


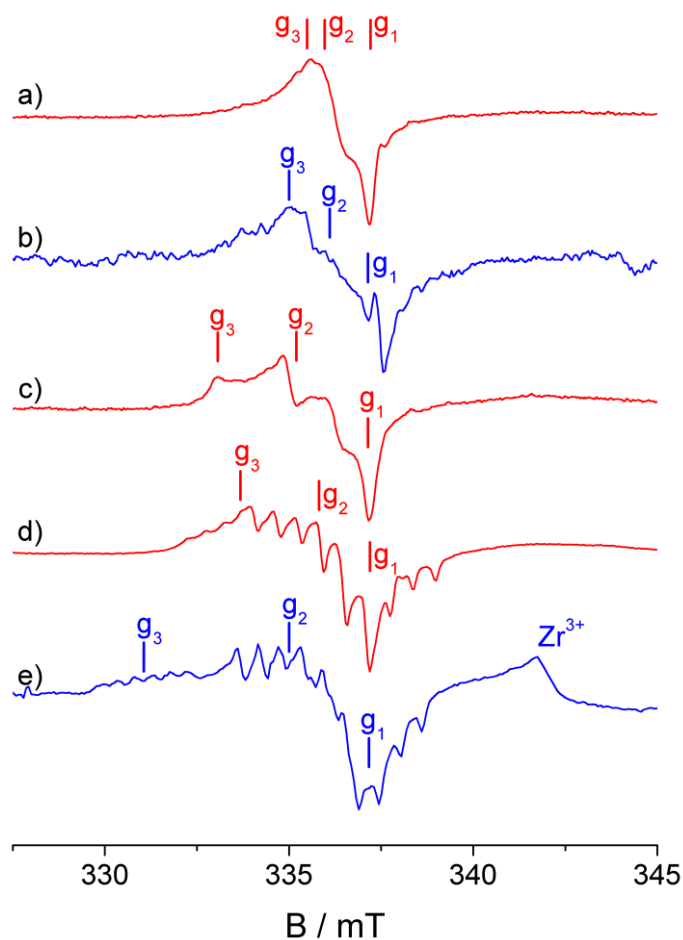Scheme 3. Model structure for a hole trapped on an oxygen ion coordinated by three metal cations.

Figure 5. EPR spectra of trapped holes (O$^{\bullet-}$) in various metaloxides. a) $TiO_2$, b) $ZrO_2$ c) surface hydrated $TiO_2$ d) Al-$TiO_2$ e) Al-$ZrO_2$.

The site undergoes a polaronic distorsion upon hole trapping. The delocalization of the unpaired electron towards Al is extremely low and the spin density results strongly localized in a *p* orbital of the oxygen [58].

### 4.2. Monitoring surface reactivity of charge carriers

The redox reactivity of electrons and holes at the surface of the photocatalyst nanoparticles is the second essential step of a photocatalytic process. A preliminary analysis of the surface reactivity can be done, using EPR, according to a procedure developed in our laboratory and consisting in the use of various irradiation sources (UV, visible light, monochromatic or polychromatic irradiation) to illuminate the solid under a gas atmosphere. In particular oxygen is used to test the reactivity of electrons in CB and hydrogen to test that of holes in VB. We note that, the test does not quantify the actual reactivity of the charge carriers that depends on the electrochemical potentials of the conduction band (electrons) or of the valence band (holes) and on the redox reaction potential of the

species in solution or in gas phase. Rather, it is aimed to establish whether the photogenerated carriers reach reactive sites at the surface of the nanoparticles since this is the required condition for further reactivity. For this reason, two gases with a strong affinity respectively for electrons ($O_2$) and holes ($H_2$) have been selected as benchmarks.

As an example in Figure 6 we report the behaviour of $ZrTiO_4$, a semiconducting solid with a band gap of about 3.8 eV under irradiation with a UV lamp [44]. The EPR spectrum in the dark, serving as a background measure, is reported in Figure 6a and shows the existence of a tiny amount of paramagnetic defects in the as-prepared solid. As discussed in the previous section UV irradiation under vacuum leads to a clear evidence of charge separation with stabilisation of a fraction of the electron and holes involved (Figure 3a and 6b). UV irradiation under $O_2$ and $H_2$ atmosphere yield the spectra reported in Figure 6c and 6d, respectively. The two results dramatically differ from each other and from what is observed after irradiation under vacuum (Figure 6b). The signal in Figure 6c shows the typical features of an adsorbed superoxide ($O_2^-$) which is characterized by a rhombic g tensor whose $g_{zz}$ component (visible at low magnetic field) has a value that depends on the nature of the adsorbing positive site [59].

The formation of superoxide takes place by one-electron reduction of molecular oxygen at the surface of the nanocrystals

$$O_{2(gas)} + e^-_{(CB)} \rightarrow O_2^- / Ti^{4+} , O_2^- / Zr^{4+} \tag{5}$$
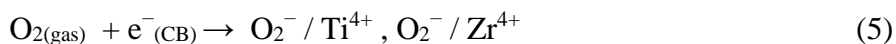
and is thus an evidence of the fact that a fraction of photogenerated electrons move to the surface reaching sites suitable to promote the reduction of gas-phase $O_2$. The two components appreciable in the $g_{zz}$ region of the signal (Figure 6c) indicate that the $O_2^-$ adsorbing sites at the solid surface are two, namely $Ti^{4+}$ ($g_{zz} = 2.022$) and $Zr^{4+}$ ($g_{zz} = 2.030$).
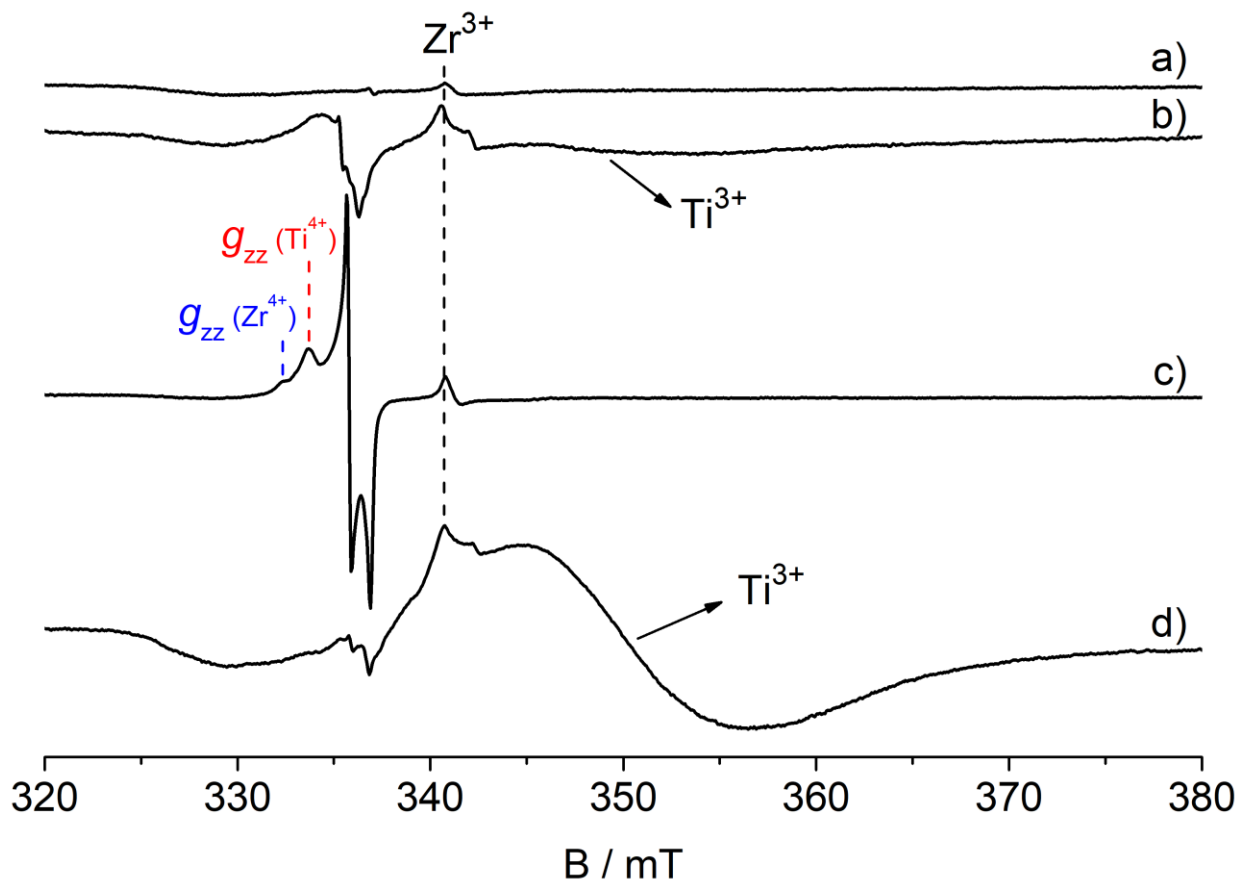
Figure 6. EPR spectra recorded upon UV irradiation of $ZrTiO_4$. a) background collected in the dark, b) irradiation under vacuum, c) under oxygen atmosphere, d) under hydrogen atmosphere

The higher abundance of $O_2^-$ / $Ti^{4+}$ species is explained in terms of the smaller size of titanium ions that exert a higher electrostatic attraction on the negative radical ion.

Figure 6d reveals the reactivity of photogenerated holes with gaseous $H_2$. Irradiation under hydrogen causes the appearance of a highly intense signal of $Ti^{3+}$ ions. Here the reaction mechanism is more complex and is based on the ability of a surface hole ($O^•$) to cause the homolytic splitting of $H_2$ generating reactive hydrogen atoms [60].

$$h^+_{(VB)} + O^{2-}_{(surf)} \rightarrow O^•_{(surf)} \qquad (6)$$

$$O^•_{(surf)} + H_{2(gas)} \rightarrow OH^-_{(surf)} + H^• \qquad (7)$$
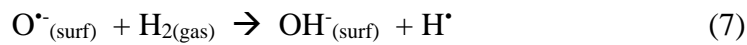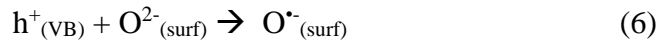
H atoms are highly reducing entities and react at the surface transferring their electron to the more reducible species of the solid, in this case, $Ti^{4+}$ ions

$$H^• + O^{2-}_{(surf)} + Ti^{4+} \rightarrow OH^-_{(surf)} + Ti^{3+} \qquad (8)$$
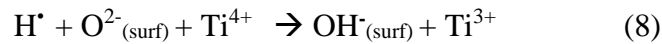
The high intensity of the $Ti^{3+}$ signal in Figure 6d is due to the combined effect of both photogenerated electrons that directly reduce $Ti^{4+}$ ions (eq. 4) and photogenerated hole that achieve the same $Ti^{4+}$ reduction through the mechanism described in Eq.s 6-8. Interestingly, the spectrum in Figure 6d does not vanish rising the temperature from 77K to room temperature (and cooling again for spectra recording in a thaw-freeze procedure) as all the photogenerated holes have been consumed by the reaction with molecular hydrogen and no electron-hole recombination can therefore occur. This experiment serves as a proof of the proposed reaction mechanism.

To summarize the data presented in this section show that CW-EPR can be applied to a preliminary screening of the photoactivity of a semiconducting system. This is particularly useful to explore the features and the potential of newly prepared system since the simple experiments described in this Section can be easily adapted to each system and performed under various irradiation conditions and provide hints about the potential catalytic activity of a given system.

### 4.3. Monitoring photogenerated radicals in solution

Photocatalytic reactions performed in aqueous solutions imply the formation of reactive radical species at the solid-liquid interface stemming from the interaction of charge carriers with water or with other molecules dissolved in the liquid medium. The most important radical species in environmental catalysis is the hydroxyl radical ($OH^•$) owing to its ability to perform total oxidation of organic pollutants. Also important, as formed by direct reduction of dissolved molecular oxygen, are the $O_2^-$ superoxide radical and its protonated form, the hydroperoxyl radical $OOH^•$ which usually coexist in equilibrium. Due to their high reactivity, the concentration of such radicals in the liquid media never reach a value high enough to permit their direct detection by EPR. This problem can be usually overcome using an EPR based technique denominated spin trapping. In short spin trapping consists in adding to the system under examination a small amount of a diamagnetic molecule (the trap) capable of reacting with the transient radical (primary radical) producing, by direct addition, a

new and more stable radical molecule, called the spin adduct [61]. The higher stability of the adducts allows accumulation of these molecules whose concentration can reach detectable values.

The most employed molecules as spin traps are aliphatic or cyclic nitrones that by direct addition of a radical $R^\bullet$ form a paramagnetic nytrosil adduct. The latter one exhibits a typical EPR spectrum whose shape varies depending on the trapped primary radical. The most popular spin trap in photocatalysis research is the 5,5-dimethyl-1-pyrrolyne *N*-oxide or DMPO (Scheme 4) that reacts with a generic R radical according to the following scheme.
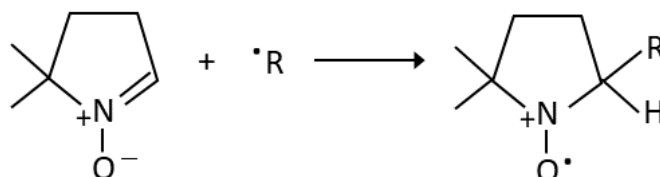


Scheme 4. Reaction between DMPO spin adduct with a R radical.

The main features of the EPR spectrum of a DMPO spin adduct are the hyperfine triplet due to $^{14}N$ (I=1) and the doublet due to $^{1}H$ (I=1/2) in position 2 ($H_\beta$) both sensitive to the nature of the incoming R radical (Scheme 4). The EPR spectrum the DMPO adduct can thus be used to unravel the nature of the R radical and for quantitative evaluations of the radical concentration. Scheme 5 shows the spin adducts formed upon reaction of DMPO with $OH^\bullet$ and $O_2^{-\bullet}$ radicals respectively
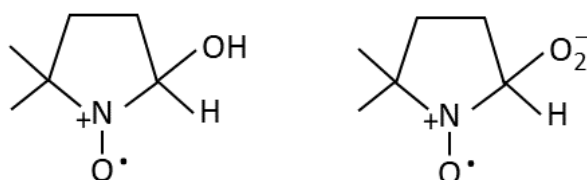


Scheme 5. Spin adducts formed upon reaction of DMPO with $OH^\bullet$ (left side) and $O_2^{-\bullet}$ radicals (right side)
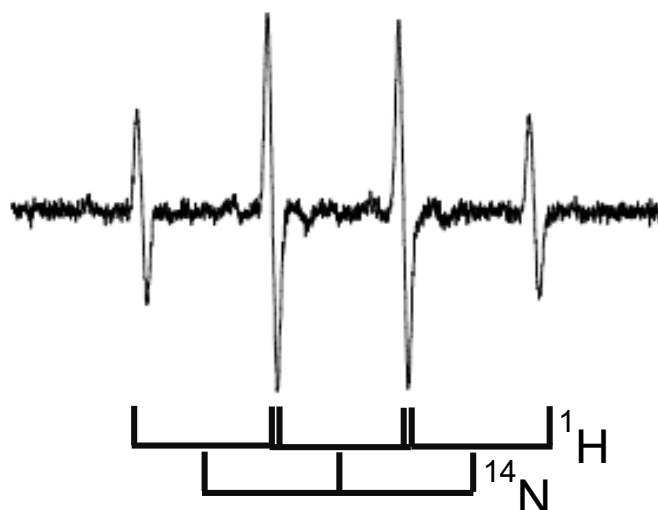
Figure 7.  EPR spectrum and related stick diagram of a DMPO-OH adduct.

In the former case the hyperfine parameters are $a_N$= 1.5mT and $a_H$ = 1.5mT. The fortuitous coincidence of the two $a_{iso}$ values gives to the spectrum the typical structure of a quartet with 1:2:2:1 intensity ratio. Figure 7 reports the typical spectrum of a DMPO-OH spin adduct and the related stick diagram that clarify the origin of the spectral structure.

In the second case the parameters of the DMPO-$O_2^-$ spin adduct are about $a_N$= 1.43mT and $a_H$ = 1.17mT. A third weaker H interaction due to the H in $\gamma$ position is also visible with $a_H$ = 0.12mT (Figure 8, the stick diagram reports the two main interactions only)
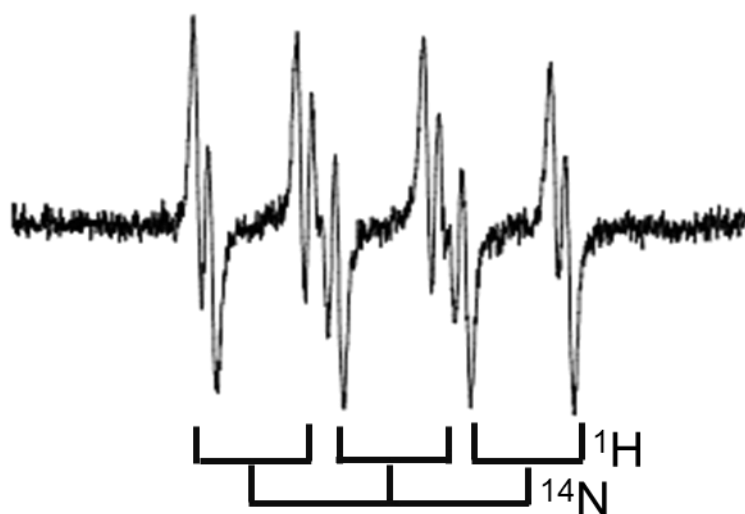


Figure 8.  EPR spectrum and related stick diagram of a DMPO-OOH adduct.

A typical example of spin trapping experiment aimed to monitor the concentration of OH˙ radicals as a function of the irradiation conditions is reported in Figure 9. In the experiment an aqueous suspension of titanium dioxide is irradiated with a lamp emitting UV and visible frequencies. The EPR spectra are recorded at suitable time intervals. The intensity of the spectra (Figure 9 b) is evaluated via double integration of the first derivative signals in Figure 9 and the corresponding spin concentration can be derived comparing the integrated intensities with those of standard solutions of a stable radical, usually 2,2-diphenyl-1-picrylhydrazyl (DPPH). Similar diagrams are usually compared to monitor the ability of the system to produce OH˙ (or other radicals) under irradiation since this feature is reasonably proportional to its actual photocatalytic activity in reactions involving the radical itself. As a word of caution, we stress that spin-trapping is a simple and effective method, however care should be exerted in interpreting the results. Given that only spin-adducts and not primary radicals are detected, the lifetime and trapping efficiency of each adduct should be assessed when multiple radicals are formed and quantification is attempted. Moreover, the spin-trap itself may be prone to photo-degradation under intense light yielding paramagnetic by-products that could be mistaken for genuine catalytic intermediates, therefore thorough cross-checking and control experiments are needed.
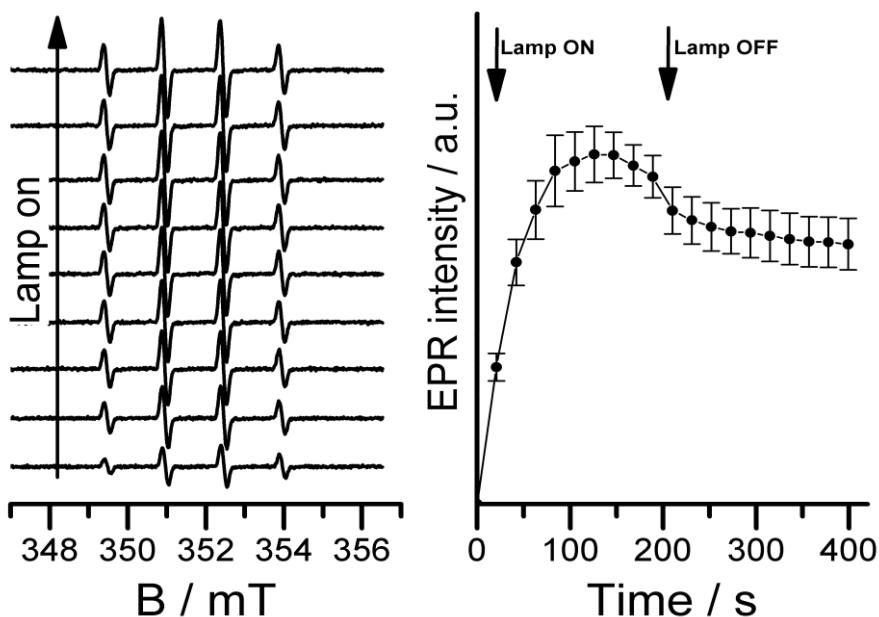
Figure 9. EPR spectra of DMPO-OH adducts in a suspension of irradiated $TiO_2$ (a)recorded as a function of irradiation time. In (B) the corresponding quantitative analysis obtained by integration of the spectra.

## 5. Conclusions

To deeply understand the complexity of photocatalytic phenomena a variety of experimental and computational tools are clearly necessary. In the present contribution we have shown how Electron Magnetic Resonance techniques, and in particular the widely available CW-EPR can contribute to monitor essential steps of the whole photocatalytic process. These can be directly monitored taking advantage of the fact that electron magnetic spectroscopy exploits microwave frequencies that do not interfere with the UV, visible and IR radiation used in photocatalytic studies. EPR can thus easily be performed   both in the dark and under illumination providing description of both ground and excited states of the system under investigation.

In the examples reported above we have described the role of EPR in characterizing the paramagnetic defects that are nearly always present in a photocatalytic material. In some cases, point defects in the solid bring about desirable properties for instance the sensitisation of a material to frequencies in the visible range; in other cases, they are detrimental towards activity since they may favour recombination of charge carriers. We have also shown how the processes of charge carriers stabilisation, migration and reactivity can be followed by EPR since the one-electron transfer typical of photocatalytic mechanism naturally lead to the formation of paramagnetic entities. When the investigation of the reactivity is extended beyond the solid surface the difficulties grows, as it is not trivial to monitor highly reactive species like radical intermediates formed in solution. However, EPR provides a nearly unique tool to monitor such reactive intermediates in solution exploiting the spin trapping techniques that deliver indirect, however valuable, information about the nature and amount of such elusive species.

## Acknowledgments

## References

[1]     Hoffmann M R, Martin S T, Choi W and Bahnemann D W 1995 Environmental applications of semiconductor photocatalysis *Chem. Rev.* **95** 69-96

[2]     Hashimoto K, Irie H and Fujishima A 2005 $TiO_2$ photocatalysis: A historical overview and future prospects *Jpn. J. Appl. Phys., Part 1* **44** 8269-85

[3]     McKone J R, Lewis N S and Gray H B 2014 Will solar-driven water-splitting devices see the light of day? *Chem. Mater.* **26** 407-14

[4]     Hisatomi T, Kubota J and Domen K 2014 Recent advances in semiconductors for photocatalytic and photoelectrochemical water splitting *Chem. Soc. Rev.* **43** 7520-35

[5]     Lubitz W 2004 *EPR in Photosynthesis* in *Electron Paramagnetic Resonance. A Specialist Periodical Report,* ed Royal Society of Chemistry Gilbert, B., Davies, M., Murphy, D., Cambridge, U.K. 174–242

[6]     Carbonera D 2009 *Electron Paramagnetic resonance in Biochemistry and Biophysics. Part II. Photosynthesis. in Electron Paramagnetic Resonance. A practitioner toolkit.,* ed J. Wiley and sons Brustolon M., Giamello E., Hoboken NY. 403-25

[7]     Hoff A J 1987 *Electron paramagnetic resonance in photosynthesis* in *New Compr. Biochem.,* ed Elsevier Amesz J. 97-123

[8]     Howe R F and Gratzel M 1985 EPR observation of trapped electrons in colloidal titanium dioxide *J. Phys. Chem.* **89** 4495-9

[9]     Rajh T, Ostafin A E, Micic O I, Tiede D M and Thurnauer M C 1996 Surface modification of small particle $TiO_2$ colloids with cysteine for enhanced photochemical reduction: an EPR study *J. Phys. Chem.* **100** 4538-45

[10]    Coronado J M, Maira A J, Conesa J C, Yeung K L, Augugliaro V and Soria J 2001 EPR study of the surface characteristics of nanostructured $TiO_2$ under UV irradiation *Langmuir* **17** 5368-74

[11]    Hurum D C, Agrios A G, Gray K A, Rajh T and Thurnauer M C 2003 Explaining the enhanced photocatalytic activity of Degussa P25 mixed-phase $TiO_2$ using EPR *J. Phys. Chem. B* **107** 4545-9

[12]    Yang S, Halliburton L, Manivannan A, Bunton P, Baker D, Klemm M, Horn S and Fujishima A 2009 Photoinduced electron paramagnetic resonance study of electron traps in $TiO_2$ crystals: oxygen vacancies and $Ti^{3+}$ ions *Appl. Phys. Lett.* **94** 162114

[13]    Priebe J B, Karnahl M, Junge H, Beller M, Hollmann D and Brückner A 2013 Water reduction with visible light: synergy between optical transitions and electron transfer in Au-$TiO_2$ catalysts visualized by in situ EPR spectroscopy *Angew. Chem. Int. Ed.* **52** 11420-4

[14]    Chiesa M, Giamello E and Che M 2010 EPR characterization and reactivity of surface-localized inorganic radicals and radical ions *Chem. Rev.* **110** 1320-47

[15]    Seidel H and Wolf H 1968 *ESR and ENDOR Spectroscopy of Color Centers in Alkali Halide Crystals* in *Physics of Color Centers,* ed Academic Press W. B. Fowler, New York, NY, U.S.A.

[16]    Spaeth J M and Overhof H 2013 *Point defects in semiconductors and insulators* vol 51 ed Springer Science & Business Media, Berlin

[17]    Asahi R, Morikawa T, Ohwaki T, Aoki K and Taga Y 2001 Visible-light photocatalysis in nitrogen-doped titanium oxides *Science* **293** 269-71

[18]     Asahi R, Morikawa T, Irie H and Ohwaki T 2014 Nitrogen-doped titanium dioxide as visible-light-sensitive photocatalyst: designs, developments, and prospects *Chem. Rev.* **114** 9824-52

[19]     Livraghi S, Paganini M C, Giamello E, Selloni A, Di Valentin C and Pacchioni G 2006 Origin of photoactivity of nitrogen-doped titanium dioxide under visible light *J. Am. Chem. Soc.* **128** 15666-71

[20]     Livraghi S, Chierotti M R, Giamello E, Magnacca G, Paganini M C, Cappelletti G and Bianchi C 2008 Nitrogen-doped titanium dioxide active in photocatalytic reactions with visible light: a multi-technique characterization of differently prepared materials *J. Phys. Chem. C* **112** 17244-52

[21]     Irie H, Washizuka S, Yoshino N and Hashimoto K 2003 Visible-light induced hydrophilicity on nitrogen-substituted titanium dioxide films *Chem. Commun.* 1298-9

[22]     Diwald O, Thompson T L, Goralski E G, Walck S D and Yates J T 2004 The effect of nitrogen ion implantation on the photoactivity of TiO$_2$ rutile single crystals *J. Phys. Chem. B* **108** 52-7

[23]     Chen X and Burda C 2004 Photoelectron spectroscopic investigation of nitrogen-doped titania nanoparticles *J. Phys. Chem. B* **108** 15446-9

[24]     Wang Y, Feng C, Jin Z, Zhang J, Yang J and Zhang S 2006 A novel N-doped TiO$_2$ with high visible light photocatalytic activity *J. Mol. Catal. A: Chem.* **260** 1-3

[25]     Peng F, Cai L, Yu H, Wang H and Yang J 2008 Synthesis and characterization of substitutional and interstitial nitrogen-doped titanium dioxides with visible light photocatalytic activity *J. Solid State Chem.* **181** 130-6

[26]     Sakthivel S, Janczarek M and Kisch H 2004 Visible light activity and photoelectrochemical properties of nitrogen-doped TiO$_2$ *J. Phys. Chem. B* **108** 19384-7

[27]     Sato S, Nakamura R and Abe S 2005 Visible-light sensitization of TiO$_2$ photocatalysts by wet-method N doping *Appl. Catal., A* **284** 131-7

[28]     Cong Y, Xiao L, Zhang J, Chen F and Anpo M 2006 Preparation and characterization of nitrogen-doped TiO$_2$ photocatalyst in different acid environments *Res. Chem. Intermed.* **32** 717-24

[29]     Triantis T M, Fotiou T, Kaloudis T, Kontos A G, Falaras P, Dionysiou D D, Pelaez M and Hiskia A 2012 Photocatalytic degradation and mineralization of microcystin-LR under UV-A, solar and visible light using nanostructured nitrogen doped TiO$_2$ *J. Hazard. Mater.* **211-212** 196-202

[30]     Napoli F, Chiesa M, Livraghi S, Giamello E, Agnoli S, Granozzi G, Pacchioni G and Di Valentin C 2009 The nitrogen photoactive centre in N-doped titanium dioxide formed via interaction of N atoms with the solid. Nature and energy level of the species *Chem. Phys. Lett.* **477** 135-8

[31]     Barolo G, Livraghi S, Chiesa M, Paganini M C and Giamello E 2012 Mechanism of the photoactivity under visible light of N-doped titanium dioxide. Charge carriers migration in irradiated N-TiO$_2$ investigated by Electron Paramagnetic Resonance *The Journal of Physical Chemistry C* **116** 20887-94

[32]     Di Valentin C, Pacchioni G, Selloni A, Livraghi S and Giamello E 2005 Characterization of paramagnetic species in N-doped TiO$_2$ powders by EPR spectroscopy and DFT calculations *J. Phys. Chem. B* **109** 11414-9

[33]     Livraghi S, Paganini M C, Chiesa M and Giamello E 2007 Trapped molecular species in N-doped TiO$_2$ *Res. Chem. Intermed.* **33** 739-47

[34]     Polliotto V, Albanese E, Livraghi S, Pacchioni G and Giamello E 2017 The photoactive nitrogen impurity in nitrogen-doped zirconium titanate (N-ZrTiO$_4$): a combined electron paramagnetic resonance and density functional theory study *J. Mater. Chem. A* **5** 13062-71

[35]     Albanese E, Di Valentin C, Pacchioni G, Sauvage F., Livraghi S and Giamello E 2015 Nature of paramagnetic species in nitrogen-doped SnO$_2$: a combined electron paramagnetic

resonance and density functional theory study *The Journal of Physical Chemistry C* **119** 26895-903

[36]     Fittipaldi M, Gombac V, Gasparotto A, Deiana C, Adami G, Barreca D, Montini T, Martra G, Gatteschi D, Fornasiero P 2011 Synergistic role of B and F dopants in promoting the photocatalytic activity of rutile TiO2. *ChemPhysChem* **12** 2221-24.

[37]     Czoska AM, Livraghi S, Paganini MC, Giamello E, Di Valentin C, Pacchioni G 2011 The nitrogen boron paramagnetic center in visible light sensitized N-B codoped TiO$_2$. Experimental and theoretical characterisation. *Phys. Chem. Chem. Phys.***13**, 136-143

[38]     Dozzi MV, Livraghi S, Giamello E, Selli E 2011 Photocatalytic activity of S- and F- doped TiO$_2$ in formic acid mineralisation. *Photochem. Photobiol. Sci.* **10** 343-49.

[39]     Howe R F and Gratzel M 1987 EPR study of hydrated anatase under UV irradiation *J. Phys. Chem.* **91** 3906-9

[40]     Graetzel M and Howe R F 1990 Electron paramagnetic resonance studies of doped titanium dioxide colloids *J. Phys. Chem.* **94** 2566-72

[41]     Dimitrijevic N M, Saponjic Z V, Rabatic B M, Poluektov O G and Rajh T 2007 Effect of size and shape of nanocrystalline TiO$_2$ on photogenerated charges. An EPR study *J. Phys. Chem. C* **111** 14597-601

[42]     Nakaoka Y and Nosaka Y 1997 ESR investigation into the effects of heat treatment and crystal structure on radicals produced over irradiated TiO$_2$ powder *J. Photochem. Photobiol., A* **110** 299-305

[43]     Hurum D C, Gray K A, Rajh T and Thurnauer M C 2005 Recombination pathways in the Degussa P25 formulation of TiO$_2$: surface versus lattice mechanisms *J. Phys. Chem. B* **109** 977-80

[44]     Sterrer M, Berger T, Diwald O and Knözinger E 2003 Energy transfer on the MgO surface, monitored by UV−induced H$_2$ chemisorption *J. Am. Chem. Soc.* **125** 195-9

[45]     Berger T, Sterrer M, Diwald O, Knözinger E, Panayotov D, Thompson T L and Yates J T 2005 Light-induced charge separation in anatase TiO$_2$ particles *The Journal of Physical Chemistry B* **109** 6061-8

[46]     Livraghi S, Rolando M, Maurelli S, Chiesa M, Paganini M C and Giamello E 2014 Nature of reduced states in titanium dioxide as monitored by electron paramagnetic resonance. II: Rutile and brookite cases *J. Phys. Chem. C* **118** 22141-8

[47]     Polliotto V, Albanese E, Livraghi S, Indyka P, Sojka Z, Pacchioni G and Giamello E 2017 Fifty–fifty Zr–Ti solid solution with a TiO$_2$-type structure: electronic structure and photochemical properties of zirconium titanate ZrTiO$_4$ *J. Phys. Chem. C* **121** 5487-97

[48]     Livraghi S, Chiesa M, Paganini M C and Giamello E 2011 On the nature of reduced states in titanium dioxide as monitored by electron paramagnetic resonance. I: the anatase case *J. Phys. Chem. C* **115** 25413-21

[49]     Gionco C, Paganini M C, Giamello E, Burgess R, Di Valentin C and Pacchioni G 2013 Paramagnetic defects in polycrystalline zirconia: an EPR and DFT study *Chem. Mater.* **25** 2243-53

[50]     Bolis V, Fubini B, Giamello E and Reller A 1989 Effect of form of the surface reactivity of differently prepared zinc oxides *J. Chem. Soc., Faraday Trans. 1* **85** 855-67

[51]     Janotti A and Van de Walle C G 2009 Fundamentals of zinc oxide as a semiconductor *Rep. Prog. Phys.* **72** 126501

[52]     Gionco C, Paganini M C, Giamello E, Burgess R, Di Valentin C and Pacchioni G 2014 Cerium-doped zirconium dioxide, a visible-light-sensitive photoactive material of third generation *J. Phys. Chem. Lett.* **5** 447-51

[53]     Gionco C, Paganini M C, Giamello E, Sacco O, Vaiano V and Sannino D 2017 Rare earth oxides in zirconium dioxide: how to turn a wide band gap metal oxide into a visible light active photocatalyst *J. Energy Chem.* **26** 270-6

[54] Cerrato E, Gionco C, Paganini M C, Giamello E, Albanese E and Pacchioni G 2018 Origin of visible light photoactivity of the $CeO_2$/ZnO heterojunction *ACS Appl. Energy Mater.* **1** 4247-60

[55] Calza P, Gionco C, Giletta M, Kalaboka M, Sakkas V, Albanis T and Paganini M C 2017 Assessment of the abatement of acelsulfame K using cerium doped ZnO as photocatalyst *J. Hazard. Mater.* **323** 471-7

[56] Shirai K, Fazio G, Sugimoto T, Selli D, Ferraro L, Watanabe K, Haruta M, Ohtani B, Kurata H, Di Valentin C and Matsumoto Y 2018 Water-assisted hole trapping at the highly curved surface of nano-$TiO_2$ photocatalyst *J. Am. Chem. Soc.* **140** 1415-22

[57] Panarelli E G, Livraghi S, Maurelli S, Polliotto V, Chiesa M and Giamello E 2016 Role of surface water molecules in stabilizing trapped hole centres in titanium dioxide (anatase) as monitored by Electron Paramagnetic Resonance *J. Photochem. Photobiol., A* **322** 27-34

[58] Gionco C, Livraghi S, Maurelli S, Giamello E, Tosoni S, Di Valentin C and Pacchioni G 2015 Al-and Ga-doped $TiO_2$, $ZrO_2$, and $HfO_2$: the nature of O 2p trapped holes from a combined electron paramagnetic resonance (EPR) and density functional theory (DFT) study *Chem. Mater.* **27** 3936-45

[59] Chiesa M, Giamello E, Paganini M C, Sojka Z and Murphy D M 2002 Continuous wave electron paramagnetic resonance investigation of the hyperfine structure of $^{17}O_2^-$ adsorbed on the MgO surface *J. Chem. Phys.* **116** 4266-74

[60] Berger T, Diwald O, Knözinger E, Napoli F, Chiesa M and Giamello E 2007 Hydrogen activation at $TiO_2$ anatase nanocrystals *Chem. Phys.* **339** 138-45

[61] Jeong M S, Yu K-N, Chung H H, Park S J, Lee A Y, Song M R, Cho M-H and Kim J S 2016 Methodological considerations of electron spin resonance spin trapping techniques for measuring reactive oxygen species generated from metal oxide nanomaterials *Sci. Rep.* **6** 26347